

Revisiting Convolutional Neural Networks for Urban Flow Analytics

Yuxuan Liang¹, Kun Ouyang¹, Junbo Zhang², Yu Zheng², David S. Rosenblum¹

¹ School of Computing, National University of Singapore, Singapore

² JD Intelligent Cities Research & JD Intelligent Cities Business Unit, Beijing, China
{yuxliang, msjunbozhang, msyuzheng}@outlook.com
{ouyangk, david}@comp.nus.edu.sg

Abstract. Convolutional Neural Networks (CNNs) have been widely adopted in raster-based urban flow analytics by virtue of their capability in capturing nearby spatial context. By revisiting CNN-based methods for different analytics tasks, we expose two common critical drawbacks in the existing uses: 1) inefficiency in learning global context, and 2) overlooking latent region functions. To tackle these challenges, in this paper we present a novel framework entitled DeepLGR that can be easily generalized to address various urban flow analytics problems. This framework consists of three major parts: 1) a local context module to learn local representations of each region; 2) a global context module to extract global contextual priors and upsample them to generate the global features; and 3) a region-specific predictor based on tensor decomposition to provide customized predictions for each region, which is very parameter-efficient compared to previous methods. Extensive experiments on two typical urban analytics tasks demonstrate the effectiveness, stability, and generality of our framework.

Keywords: Urban Computing · Urban Flow Analytics · Convolutional Networks

1 Introduction

Urban flow analytics is very critical for smart city efforts. A unique property of the flow data is the spatio-temporal (ST) correlation: the presence of dependencies among measurements induced by the spatial and temporal dimensions.

To model this unique property of urban flow, Convolutional Neural Network (CNN) has attracted growing attention due to its success in many research fields such as computer vision. A pioneering work [24] provided a CNN-based method named DeepST for modeling citywide crowd flow, where convolution operators are used to extract spatially near and distant dependencies. ST-ResNet [23] further enhanced the predictive performance of DeepST with deep residual learning. Another work, the ConvLSTM layer [21] not only preserves the advantages of LSTM but is also suitable for ST data due to its inherent convolutional structure. Very recently, a novel ConvPlus structure in DeepSTN+ [14] was proposed to learn the global dependencies between two arbitrary regions. In addition, [13] introduced a CNN-based framework to infer fine-grained urban flows from coarse-grained inputs. These CNN-based methods are characterized by two components: a complicated ST feature learner to capture features of the measurements, and a simple task-specific predictor to output predictions on all regions. However, there are two main drawbacks in these existing approaches:

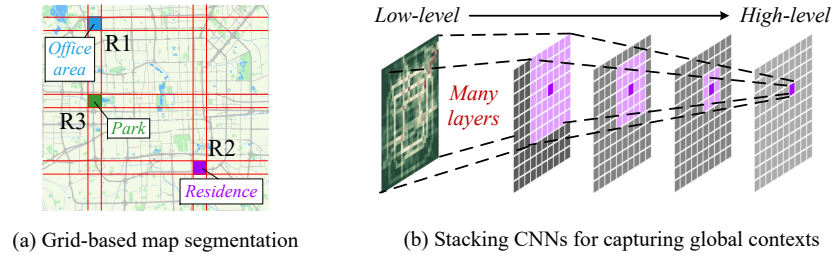


Fig. 1. Application of CNNs for urban flow analytics.

1) *Inefficiency in learning global context.* Nowadays, people can travel around a city quickly. Figure 1(a) shows an example from Beijing: when predicting the inflows of R1 (an office area) during morning hours, the information of R2 (a residential area) needs to be considered even though it is very distant from R1. Thus, capturing spatial global dependencies is of great importance to urban flow analytics. To learn global context, existing methods mainly employ two approaches:

- *Stacking convolutional layers to increase receptive fields.* Most previous studies such as DeepST and ST-ResNet employ CNNs to capture information locally, but have to stack a number of layers to capture global context as in Figure 1(b). This is very inefficient, since relationships between distant regions on the feature map can only be captured by a near-top layer with a sufficiently large receptive field to cover all the regions of interest.
- *Learning long-range spatial dependencies directly.* Instead of gradually increasing receptive fields, DeepSTN+ [14] attempts to capture global context in *every layer* using a structure named ConvPlus, which explicitly models all pairwise relationship between regions. However, a single layer of ConvPlus without pooling requires $O(n^2)$ parameters, where n is the number of regions. Assuming we partition a city into 128×128 regions evenly ($n = 16384$), the number of parameters in a ConvPlus layer already exceeds 250 million. Constrained by this bloated structure, DeepSTN+ cannot easily go deeper to learn higher-level representations for each grid. Thus, how to learn the global context in a more efficient manner still remains a challenge.

2) *Ignoring latent region functions.* Different from pixels in image processing, urban regions have different land functions according to their locations and surrounding POIs (Points of Interests) [27,16]. Recall that region R1, R2 and R3 in Figure 1 correspond to an office area, a residential area and a park zone respectively. From Figure 2(a), it can be seen easily that their daily patterns are entirely different. For instance, the office area (R1) usually reaches a traffic peak in the morning, while the residential area (R2) exhibits growth after dinner time. Figure 2(b) also shows the difference between them in terms of their inflow distribution. Accordingly, a simple predictor using shared parameters to predict all regions' flows would result in degraded performance. However, the aforementioned methods have overlooked the latent region functions that have a great impact on the spatio-temporal correlations.

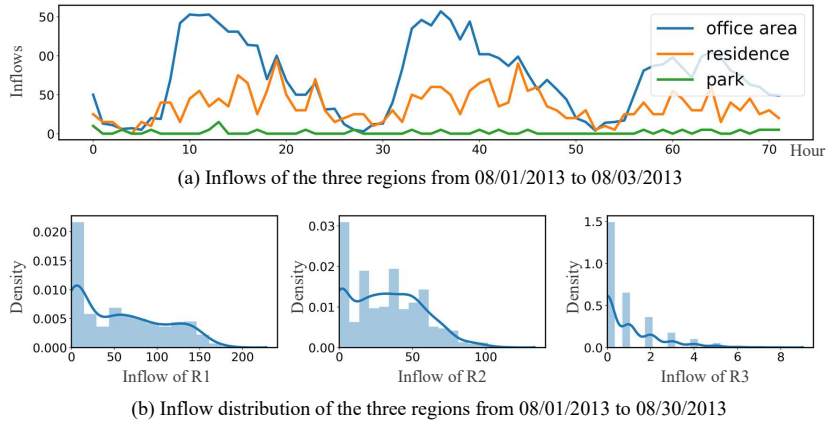


Fig. 2. Illustration of daily patterns and inflow distribution in three regions.

To address the above problems, in this paper, we make the following contributions to the community.

Primarily, we introduce DeepLGR, the first-ever general framework for raster-based urban flow analytics. It is named according to the three major procedures that it stratifies a given task: **L**ocal context extraction, **G**lobal context aggregation and **R**egion-specific prediction. Specifically,

- we present the first attempt to better model the local context (*i.e.*, features) using Squeeze-and-Excitation networks (SENet) [5], which excels by including channel-wise information as additional knowledge;
- we design an original global context module that aggregates the local representations using a specific pooling method, and then upsamples the global priors to the original scale to generate global features;
- we introduce a region-specific predictor based on tensor decomposition that factorizes the region-specific parameters of the predictor into a smaller core tensor and adjacent matrices. Compared to a previous attempt [16] using matrix factorization, our method can better learn latent region functions along with the spatial dependencies between regions while using much fewer parameters.

In addition, we evaluate our framework on two important urban flow analytics tasks: urban flow forecasting [24,23,14] and fine-grained urban flow inference [13]. Extensive experiments demonstrate the state-of-the-art performance and stability achieved by our framework. We will release code and data for public use soon.

2 Formulation

In this section, we introduce several notations and formulate the problem of urban flow analytics. In particular, we use calligraphic letters (e.g., \mathcal{X}) and bold capital letters (e.g., \mathbf{X}) to denote tensors and matrices, respectively. We employ bold lowercase letters (e.g.,

\mathbf{x}) to represent vectors, and non-bold letters (e.g., x) as scalars. As shown in Figure 1(a), we first follow the previous study [24] to partition an area of interest (e.g., a city) evenly into a $H \times W$ grid map based on longitude and latitude where a grid denotes a region. Thus, the urban flow at a certain time t can be denoted as a 3D tensor $\mathcal{P}_t \in \mathbb{R}^{H \times W \times K}$, where K is the number of different flow measurements (e.g., inflow and outflow). Each entry (i, j, k) denotes the value of the k -th measurement in the region (i, j) .

Without loss of generality, we use $\mathcal{X} \in \mathbb{R}^{H \times W \times C}$ and $\mathcal{Y} \in \mathbb{R}^{H' \times W' \times D}$ as the input and output for a urban flow analytics task, where C and D are the number of channels. For example, in the task of crowd flow forecasting [24,23,14], the input is the historical observations $\mathcal{X} = \{\mathcal{P}_i | i = 1, 2, \dots, \tau\} \in \mathbb{R}^{H \times W \times K\tau}$ and the target is to predict $\mathcal{Y} = \mathcal{P}_{\tau+1} \in \mathbb{R}^{H \times W \times K}$.

3 Methodology

Figure 3 presents the framework of DeepLGR, which can be easily generalized to all kinds of raster-based ST data. Compared to the previous methods composed of an ST feature learner and a shared predictor for all regions, our framework contains three major components: local context module, global context module and region-specific predictor. In the first component, we employ the SENet to learn local context (i.e., features) from the input tensor \mathcal{X} . To capture global context, we further design a global context module that extracts global contextual priors from the learned local representations by a specific pooling method, and upsample the priors to the original scale to generate the global features. Once we obtain features from both the local and global views, we concatenate them into a tensor and then feed it to the region-specific predictor to make customized predictions for each region respectively, denoted as \mathcal{Y} .

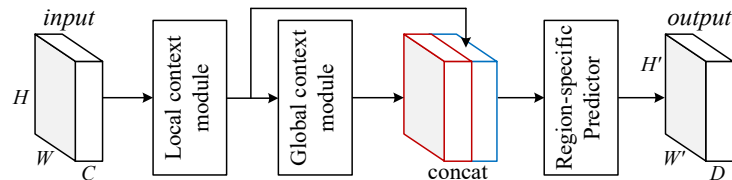


Fig. 3. The pipeline of our framework (DeepLGR), which contains three major components: i) local context module; ii) global context module; and iii) region-specific predictor.

As mentioned in Section 1, capturing the spatio-temporal property is of great importance to urban flow analytics. For spatial dependencies, our framework employ the first two components which strategically capture both local and global-level dependencies between regions. As we mainly focus on the mainstream CNN architectures for urban flow analytics rather than RNN techniques, the temporal dependencies like closeness, period and trend [23,14], if any, are considered in the channels of input. Next, we will detail the three major components in the following section respectively.

3.1 Local Context Module

Recall that both the previous and current state-of-the-arts [23,14] use residual blocks to model the spatial dependencies from nearby regions. However, these methods mainly focus on the spatial dimension and have overlooked the channel-wise information in the feature maps. Thus, we employ SENet to fuse both spatial and channel-wise information within local receptive fields at each layer, which has proven to be effective in producing compacted and discriminative features of each grid.

Figure 4(a) illustrates the pipeline of the module for local context modeling. The input is fed to a convolutional layer for initialization. Then, we stack M squeeze-and-excitation (SE) blocks in Figure 4(b) for feature extraction, which is composed of three stages: 1) a residual block [3] for feature learning; 2) a squeeze operation to squeeze global spatial information into a channel descriptor by global average pooling; 3) an excitation operation to fully capture the channel-wise dependencies: it first computes the attention coefficients over each channel via two fully connected layers followed by a sigmoid function, and then rescales the channels of original inputs by these weights. Finally, we use an output convolutional layer to transform the obtained high-level feature maps to the input of the next module. In summary, the SE structure enables this module to learn better representations for each region locally.

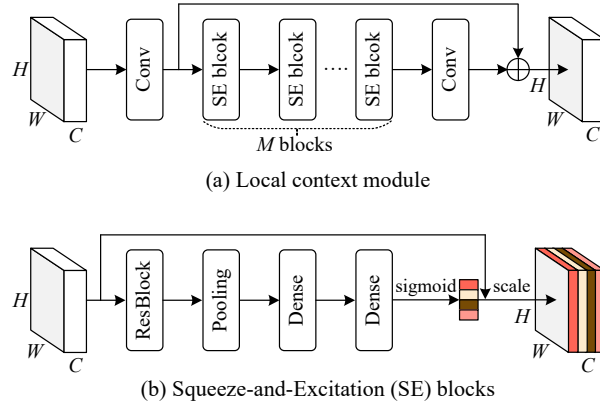


Fig. 4. The pipeline of local context module. Conv: convolution. ResBlock: Residual block. Pooling: global average pooling. Dense: fully connected layer.

3.2 Global Context Module

After modeling local context, we design a specific module that takes the output of the former component as input to learn global context. As depicted in Figure 5, we first employ the spatial pyramid pooling [2] to generate a set of the global priors, where each prior is a spatially abstract of the original input under different pyramid scales. This operation allows the module to separate the feature map into different sub-regions

and build pooled representation for different locations. For example, the 1×1 prior (the red cube) denotes the coarsest level with only one single value at each channel, which is equivalent to the global pooling operation that covers the whole image. In this study, we use a 4-level pyramid (1×1 , 2×2 , 4×4 and 8×8) to squeeze the input by average pooling.

Once the global priors are obtained, an 1×1 convolution layer followed by a Batchnorm layer [7] are used for dimension reduction of channels (from N to $N/8$). Inspired by the study [13] aiming at inferring fine-grained crowd flow from coarse-grained counterparts, we employ the Subpixel block [17] to upsample the priors to generate new representations with the same size as the original inputs. Different from the previous study [25] using bilinear interpolation for upsampling the priors, the Subpixel block considers the relationship between a super-region and its corresponding sub-regions by introducing a parametric design. Finally, we concatenate the module input (*i.e.*, local context) with all levels of global features (*i.e.*, global context) as the output of this module.

Compared to the previous attempt (ConvPlus [14]) for learning global dependencies, our solution is more efficient and lightweight. Each ConvPlus layer directly models the pairwise relationships among all regions, thus demanding $O(n^2)$ parameters. With the increase of spatial granularity, it will induce extremely high computational costs due to the massive parameters. Therefore, DeepSTN+ can hardly learn higher-level representations by simply increasing network depth. On the contrary, as we have separated the procedures of local and global context modeling, we can easily increase the network depth to gain better capacity.

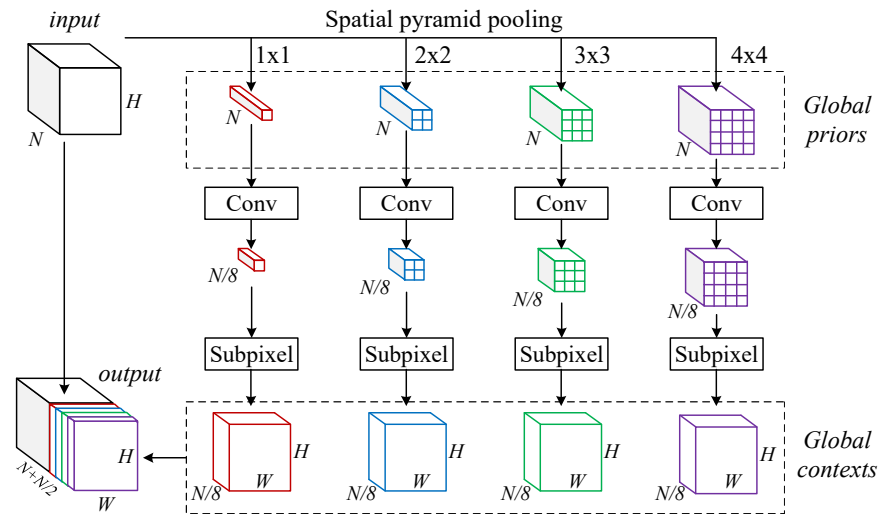


Fig. 5. The pipeline of global context module, where Conv denotes a 1×1 convolutional layer for dimension reduction, and Subpixel contains a convolutional layer and a pixelshuffle operation sequentially to upsample the contextual priors. For simplicity, we use a 4-level pyramid (1×1 , 2×2 , 3×3 and 4×4) for an illustration.

3.3 Region-Specific Predictor

As mentioned before, each urban region has its unique land function. Previous studies [24,23,14] mainly employ a single fully connected layer (equivalent to a 1×1 convolution) with shared weights as the predictor for all regions, which fails to capture this critical property. Thus, it is necessary to assign region-specific predictor to each region.

Recall that the high-level feature obtained from last module is $\mathcal{Z} \in \mathbb{R}^{H \times W \times N'}$ and prediction result is $\mathcal{Y} \in \mathbb{R}^{H \times W \times D}$, where $N' = N + N/2$. Conventionally, the number of parameters in a shared fully connected layer is $n_f = N'D$. To achieve region-specific predictor, an intuitive solution is to use a customized fully connected layer for each region. However, it will induce $HW \times n_f$ parameters (denoted as a tensor $\mathcal{W} \in \mathbb{R}^{H \times W \times n_f}$), which can easily bloat up as the granularity increases. Recently, matrix factorization (MF) was used to avoid these drawbacks [16], in which the parameter tensor \mathcal{W} is reshaped to a matrix $\mathbf{W} \in \mathbb{R}^{HW \times n_f}$. As shown in Figure 6(a), the authors from [16] decompose the weight matrix \mathbf{W} into two *learnable* low-rank matrices, *i.e.*, region embedding matrices $\mathbf{L} \in \mathbb{R}^{k \times n_f}$ and parameter embedding matrices $\mathbf{R} \in \mathbb{R}^{HW \times k}$. With the usage of MF, the number of the predictor parameters can be reduced to $(HW + n_f)k$, where $k \ll n_f$ and $k \ll HW$.

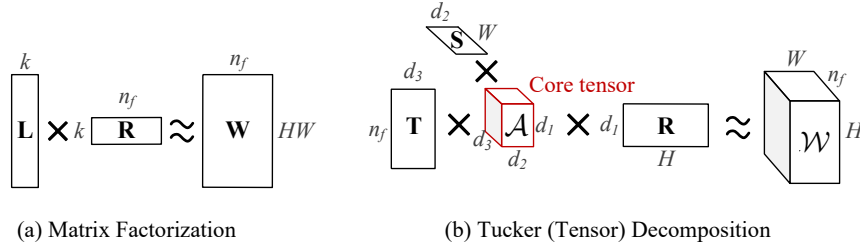


Fig. 6. Illustration of matrix factorization and tensor decomposition.

Nonetheless, directly flattening the parameter tensor \mathcal{W} over the region dimension will lose the Euclidean structure of the flow map³. Instead, we present a new idea for decomposing \mathcal{W} using tensor decomposition (TD) [20]. As illustrated in Figure 6(b), tensor \mathcal{W} is decomposed into the multiplication of a core tensor $\mathcal{A} \in \mathbb{R}^{d_1 \times d_2 \times d_3}$ and three adjoint matrices, where d_1 , d_2 , and d_3 denote the number of latent factors for each matrix. The computation is as follows:

$$\mathcal{W} = \mathcal{A} \times_R \mathbf{R} \times_S \mathbf{S} \times_T \mathbf{T}, \quad (1)$$

where \times_R stands for the tensor-matrix multiplication; the subscript R is the corresponding mode of the multiplication. For instance, $\mathbf{H} = \mathcal{A} \times_R \mathbf{R}$ is $\mathbf{H}_{ijk} = \sum_{i=1}^{d_1} A_{ijk} \times R_{ij}$. By this, we have changed the optimization target from \mathcal{W} to the core tensor \mathcal{A} as well as the three learnable matrices \mathbf{R} , \mathbf{S} and \mathbf{T} . The core tensor is a low-rank representation

³ For example, two near regions should have similar weights.

summarising both the parametric and spatial information of the origin tensor \mathcal{W} . Compared to MF-based solution [16], our tensor decomposition can handle the higher-order relationships within the parameters. In addition, the number of parameters required is $d_1d_2d_3 + d_1H + d_2W + d_3n_f$. Since d_1 , d_2 and d_3 are usually very small, TD can achieve even much fewer parameters than MF, which is validated in our experiments.

3.4 Optimization

Since our framework is smooth and differentiable everywhere, it can be trained via the back-propagation algorithm. During the training phase, we use Adam optimizer [9] to train our model by minimizing the entry-wise mean absolute error (MAE) between our prediction $\hat{\mathcal{Y}}$ and the corresponding ground truth \mathcal{Y} :

$$\mathcal{L}(\Theta) = \left\| \mathcal{Y} - \hat{\mathcal{Y}} \right\|_1 \quad (2)$$

where Θ denotes all learnable parameters in our framework.

4 Experiments

To validate the generality of DeepLGR, we conduct experiments on two typical tasks of urban flow analytics:

- *Crowd flow forecasting*: This task is to forecast the future crowd flow of each region in a city from historical readings. Following the study [23], we consider the temporal dependencies (*i.e.*, closeness, period and trend) in different channels of input, and the output is the prediction of flow volume at the next timestamp.
- *Fine-grained flow inference*: In this task, we aim to infer fine-grained crowd flows throughout a city based on coarse-grained observations (*i.e.*, the output scales $H' \times W'$ is larger than the input $H \times W$). We extend the state-of-the-art method named UrbanFM [13] using our framework. Specifically, we replace the ResNet-based feature extraction of UrbanFM by our local context module. Then, we add the global context module and region-specific predictor after the subpixel blocks in UrbanFM.

4.1 Experimental Settings

Datasets Two datasets were used in our experiments, including TaxiBJ and HappyValley. The former is the fine-grained version of the ones used by [23] and the latter is provided from [13]. Specifically, TaxiBJ consists of four different time spans (denoted as P1 to P4), which derives from the trajectories of over 30,000 taxicabs, while HappyValley is the hourly observations of human flow in a theme park in Beijing from ten months. The statistics and related external factors of them are detailed in Table 1.

Using both datasets, we evaluate our framework over the two aforementioned tasks: In the first task, we employ the first 80% data as training set, the next 10% as validation set and the rest for test set; In the second task, we follow all the experiment settings of [13], including training, validation and test set partition. The upscaling factors in TaxiBJ and HappyValley are 4 and 2 respectively. To speed up the convergence of our method, a unique data normalization method [13] was applied in our study.

Table 1. Dataset description.

Dataset	TaxiBJ	HappyValley
Data type	Taxicab trip	Human flow
Resolution	(128, 128)	(50,100)
Sampling rate	30 minutes	1 hour
Time Span (mm/dd/yyyy)	P1: 07/01/2013-10/31/2013 P2: 02/01/2014-06/30/2014 P3: 03/01/2015-06/30/2015 P4: 11/01/2015-03/31/2016	01/01/2018- 10/31/2018
External factors	Meteorology, time, holiday and events	

Evaluation Metrics We employ two widely-used criteria to evaluate our model, including mean absolute error (MAE) and symmetric mean absolute percentage error (SMAPE). They are defined as:

$$\text{MAE} = \frac{1}{z} \sum_{i=1}^z |y_i - \tilde{y}_i|, \quad \text{SMAPE} = \frac{1}{z} \sum_{i=1}^z \frac{|y_i - \tilde{y}_i|}{|y_i| + |\tilde{y}_i|},$$

where y and \tilde{y} are and ground truth and predicted value respectively; z is the total number of all entries. Smaller metric scores indicate better model performances.

Baselines In the first task, we compare our framework with heuristics, time series methods and CNN-based baselines. Specifically, an intuitive method (**Last**) simply uses the last observation as the prediction result, and another heuristic (**CA**) leverages the closeness property to predict the future crowds by averaging the values from the previous 5 time steps. **ARIMA** is a well-known model for forecasting future values in a time series. Besides, the CNN-based baselines (including **DeepST** [24], **ST-ResNet** [23], **ConvLSTM** [17] and **DeepSTN+** [14]) have been introduced in Section 1.

The second task was introduced only very recently by [13], where the authors presented the state-of-the-art method named **UrbanFM**. It considers the unique characteristics of this task, including the spatial hierarchy and external factors. Other strong baselines included in this work are related to image super-resolution, such as **VDSR** [8] and **SRRResNet** [11]. As the names suggest, VDSR first used a very deep CNN for image super-resolution while SRRResNet enhanced VDSR by using the residual architecture. We mainly use these three baselines for model comparison in this task. It is worth noting that all baselines are implemented with their default settings in both tasks.

Training Details & Hyperparameters Our framework, as well as above baselines, are fully implemented by Pytorch 1.1.0 with one GTX 2080TI GPU. During the training phase, the learning rate is 0.005 and the batch size is 16. For the number of stacked SE blocks (denoted as M) in local context module, we conduct a grid search over $\{3, 6, 9, 12\}$. For simplicity, we use the same hidden dimensionality (*i.e.*, number of channels) at each SE block, and conduct a grid search over $F = \{32, 64, 128\}$. The setting in which $M = 9$ and $F = 64$ outperforms the others in the validation set. In addition, we set $d_1 = d_2 = 32$ and $d_3 = 16$ in the region-specific predictor.

4.2 Results on Crowd Flow Forecasting

Model Comparison In this section, we compare our framework with the baselines over the two datasets. We report the result of DeepLGR with $M = 9$ and $F = 64$ as our default setting. Further experiments regarding different M will be discussed later.

Table 2 shows the results over P1 to P4 in TaxiBJ. We can observe that our framework clearly outperforms all baselines over both metrics. For instance, DeepLGR shows 10.2% and 44.1% improvements on MAE and SMAPE beyond the state-of-the-art method (DeepSTN+) in P4. The conventional model ARIMA performs much worse than deep learning models in these datasets, since it only considers the temporal dependencies among time series. Apart from the CNN-based methods, ConvLSTM advances DeepST and ST-ResNet because of the positive effect of its LSTM structure. However, it overlooks the global dependencies between regions, which leads to inferiority compared to DeepSTN+ and DeepLGR. Another interesting observation is that the heuristics including CA and Last achieves much less SMAPE than previous CNN-based methods. Recall that SMAPE prefers to penalize the errors in regions with lower flow volume. This observation reveals the importance of the temporal dependencies in such regions since CA and Last only consider the temporal closeness for forecasting. Only our method performs better than the heuristics on SMAPE with the usage of tensor decomposition, which will be detailed in the ablation study. Last but not least, DeepLGR is also more stable than the baselines according to the standard deviation observations.

Table 2. Prediction results on TaxiBJ over different time spans (P1-P4), where the bold number indicates the best performance of the column. We train and test each method five times, and present results using the format: “mean \pm standard deviation”.

Method	P1		P2	
	MAE	SMAPE	MAE	SMAPE
CA	3.43	0.290	4.23	0.288
Last	3.39	0.242	4.09	0.241
ARIMA	3.08	0.403	3.53	0.385
DeepST	2.59 \pm 0.05	0.41 \pm 0.01	2.94 \pm 0.05	0.39 \pm 0.01
ST-ResNet	2.53 \pm 0.05	0.38 \pm 0.05	2.93 \pm 0.06	0.34 \pm 0.07
ConvLSTM	2.42 \pm 0.02	0.41 \pm 0.01	2.77 \pm 0.01	0.39 \pm 0.01
DeepSTN+	2.33 \pm 0.04	0.35 \pm 0.08	2.67 \pm 0.02	0.32 \pm 0.05
DeepLGR	2.15 \pm 0.00	0.19 \pm 0.00	2.46 \pm 0.00	0.18 \pm 0.00

Method	P3		P4	
	MAE	SMAPE	MAE	SMAPE
CA	4.17	0.286	2.81	0.286
Last	4.07	0.240	2.82	0.239
ARIMA	3.68	0.363	2.61	0.420
DeepST	2.97 \pm 0.04	0.39 \pm 0.01	2.16 \pm 0.04	0.43 \pm 0.02
ST-ResNet	2.91 \pm 0.06	0.33 \pm 0.05	2.15 \pm 0.04	0.32 \pm 0.06
ConvLSTM	2.87 \pm 0.01	0.39 \pm 0.01	2.09 \pm 0.02	0.43 \pm 0.02
DeepSTN+	2.82 \pm 0.04	0.38 \pm 0.05	2.05 \pm 0.01	0.34 \pm 0.05
DeepLGR	2.56 \pm 0.02	0.19 \pm 0.04	1.84 \pm 0.01	0.19 \pm 0.00

Table 3. Prediction results of various methods on the HappyValley dataset, where #Params is the number of parameters in a model and M denotes million. We train and test each method five times, and present results using the format: “mean \pm standard deviation”.

Method	#Params	MAE	SMAPE
CA	x	2.23	0.46
Last	x	2.20	0.38
ARIMA	0.00M	2.14	0.47
DeepST	0.59M	2.02 \pm 0.05	0.56 \pm 0.05
ST-ResNet	2.73M	1.98 \pm 0.05	0.53 \pm 0.04
ConvLSTM	5.98M	1.86 \pm 0.01	0.48 \pm 0.10
DeepSTN+	15.70M	1.92 \pm 0.01	0.54 \pm 0.06
DeepLGR	0.97M	1.84 \pm 0.01	0.40 \pm 0.02

Compared to TaxiBJ with a citywide scale, HappyValley focuses on a local area with a highly skewed flow distribution, where only a few regions contain dense populations. Table 3 presents a comprehensive comparison of each model over this dataset. First, it can be seen easily that our framework shows great superiority against the CNN-based methods and slightly outperforms ConvLSTM in terms of both metrics, while using as little as 6.2% of the amount of parameters required in the state-of-the-art method (DeepSTN+). This fact demonstrates that our model are more practical than other CNN-based solutions in real-world systems. Second, similar to the results in TaxiBJ, DeepLGR performs more stable than the baselines according to the standard deviation in multiple experiments. Third, the heuristic method (Last) achieves the lowest SMAPE but the second highest MAE, which can prove the skew distribution of this dataset. Last, the fact that DeepLGR and DeepSTN+ outperform ST-ResNet verifies the necessity of modeling global context in such a small area.

Ablation Study To further investigate the effectiveness of each component, we compare DeepLGR with its variants over TaxiBJ-P1. For simplicity, we use the terms as local, global and TD to denote the three components in our framework respectively. Based on them, our framework and its variants can be denoted as follows:

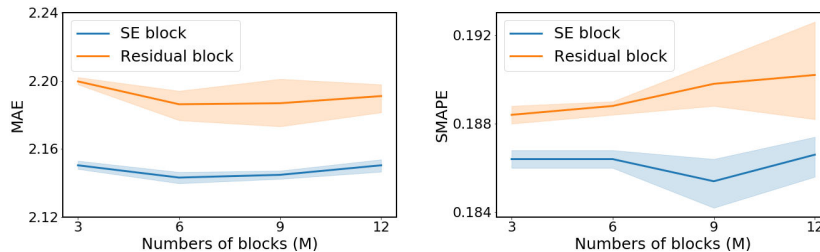
- **local+global+TD**: The original implementation of DeepLGR.
- **local+global+MF**: To show the effectiveness and lightweight property of TD against MF, we replace TD in the region-specific predictor by MF.
- **local+global**: Similar to the CNN-based baselines [24,23,14], this variant uses shared parameters (*i.e.*, not region-specific) as the predictor.
- **local+TD**: It represents the variant of DeepLGR without global context module.
- **local+MF**: We first remove global context module from DeepLGR and then replace TD in region-specific predictor by MF.
- **local+bilinear**: In this variant, we employ bilinear interpolation rather than Subpixel block to upsample the global priors, so as to obtain new global representations.
- **local**: The last two components are removed from DeepLGR, *i.e.*, we only use local context module to predict the future flow.

Table 4. Prediction results of variants over TaxiBJ-P1, where #Params is the number of parameters in a model and M denotes million. Each variant has been trained and tested five times.

Variants	#Params	MAE	SMAPE
local	0.72M	2.21 ± 0.01	0.37 ± 0.03
local+MF	0.89M	2.19 ± 0.02	0.36 ± 0.03
local+TD	0.74M	2.19 ± 0.01	0.32 ± 0.03
local+bilinear	0.73M	2.20 ± 0.02	0.35 ± 0.03
local+global	2.30M	2.17 ± 0.02	0.29 ± 0.03
local+global+MF	2.46M	2.15 ± 0.00	0.27 ± 0.01
local+global+TD	2.31M	2.15 ± 0.00	0.19 ± 0.00

Table 4 illustrates the variant comparison over TaxiBJ-P1. We discuss the effects of each model component as follows:

- *Local context module*: A powerful ST feature extractor enables the capability of extracting useful representations for each region. Compared to previous attempts like ST-ResNet based on residual blocks, our local context module largely improves the predictive performance (e.g., local vs. ST-ResNet in Table 2 and 4). We further investigate the effects of the number of SE blocks in this module. As shown in Figure 7, it achieves the best performance when $M = 6$ in the test set. Noted that we choose $M = 9$ as the default setting of DeepLGR because of its best performance on the validation set rather than the test set. Besides, we also replace the SE blocks in this module by residual blocks to show their advantages.
- *Global context module*: As a vital component in our framework, this module provides the global information to boost the performance. As illustrated in Table 4, the comparison between local and local+global (also local+TD and local+global+TD) can verify the effectiveness of this module. With the usage of Subpixel block with a parametric design, local+global brings an improvement beyond local+bilinear.
- *Region-specific predictor*: This module is used to determine the region-specific parameters for predictions. Thus, we compare it with a shared fully connected layer with n_f parameters (local+global), and the matrix decomposition method. From Table 4, we observe that TD demonstrates very competitive accuracy while using as little as 6.3 % of the number of parameters required in MF. Moreover, TD significantly outperforms MF over SMAPE since it allows the model to capture spatial dependencies between regions.

**Fig. 7.** SE block vs. residual block over P1, where the shade area denotes the standard deviation.

4.3 Results on Fine-grained Flow Inference

Experimental results on the second task (fine-grained flow inference) demonstrate the superiority of our framework again. From Table 5, we have the following observations: 1) UrbanFM equipped with our framework (denoted as local+global+TD) shows considerable improvements against its original version on both datasets, validating its great generality in different applications. For example, DeepLGR achieves 5.8% lower MAE and 28.0% lower SMAPE than UrbanFM in TaxiBJ-P1 dataset. 2) The three components of DeepLGR are effective according to the advancement of performance (only except local vs. UrbanFM in HappyValley). 3) Compared to VDSR and SRResNet for image-resolution, UrbanFM outperforms them by considering the domain knowledge, *i.e.*, spatial hierarchy and external influence [13]. From above discussions, we can see that existing approaches like UrbanFM can be easily integrated with our framework.

Table 5. Results of various models for fine-grained flow inference. We train and test each method five times, and present results using the format: “mean \pm standard deviation”.

Method	TaxiBJ-P1		HappyValley	
	MAE	SMAPE	MAE	SMAPE
VDSR	2.23 \pm 0.05	0.54 \pm 0.03	2.13 \pm 0.04	0.61 \pm 0.02
SRResNet	2.20 \pm 0.05	0.52 \pm 0.03	1.89 \pm 0.05	0.61 \pm 0.03
UrbanFM	2.07 \pm 0.03	0.25 \pm 0.02	1.80 \pm 0.02	0.41 \pm 0.02
local	1.98 \pm 0.01	0.20 \pm 0.01	1.83 \pm 0.01	0.43 \pm 0.01
local+global	1.96 \pm 0.00	0.20 \pm 0.01	1.78 \pm 0.01	0.38 \pm 0.01
local+global+TD	1.95 \pm 0.00	0.18 \pm 0.01	1.76 \pm 0.01	0.35 \pm 0.00

We further investigate the efficiency of DeepLGR. Figure 8 plots the MAE on the validation set during the training phase using TaxiBJ-P1. Remarkably, UrbanFM and DeepLGR converge much smoother and faster than the others as shown in Figure 8(a). A more detailed comparison between UrbanFM and DeepLGR lies in Figure 8(b). From this figure, we can see that DeepLGR converges at iteration 3540 (epoch 37) while UrbanFM early-stops at iteration 7720 (epoch 81). This fact demonstrates that our framework can also accelerate the training phase of existing method.

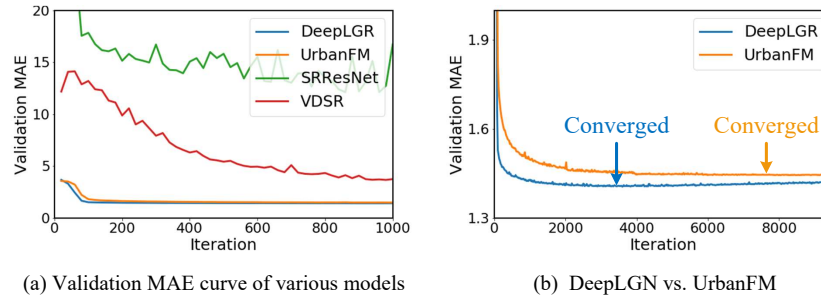


Fig. 8. Convergence speed of various methods over P1.

5 Related Work

5.1 Urban Flow Analytics

Urban flow analytics has attracted considerable attention of researchers in recent years. Zheng et al. first presented a new paradigm for trajectory data modeling [26], such as transforming trajectories data into the format of graphs or tensors, to which more machine learning and data mining techniques can be effectively applied. Inspired by this study, a series of studies explored forecasting millions or even billions of individual mobility traces [19,1]. Different from analyzing crowd behaviors on an individual level, several works started to forecast citywide traffic flows by aggregating the crowds into corresponding regions [12,4]. Among them, statistical learning was employed to capture the region-wise relationship so as to improve the predictive performance. With interests in obtaining fine-grained regional data, several studies [13,28,15] presented techniques to recover fine-grained population distribution or crowd flows given the corresponding coarse-grained inputs.

Recently, with the development of deep learning techniques, there have been many attempts focusing on end-to-end solutions for urban flow analytics. A pioneering study by [24] presented a general framework based on deep neural networks for citywide crowd flow prediction. By using a CNN architecture, their method can capture the spatio-temporal correlations reasonably and accurately. To overcome the gradient vanishing and exploding problem, they further integrated their framework with deep residual learning to collectively predict inflow and outflow of crowds in every city grid [23]. Similar insight has been applied in taxi demand prediction. For example, Yao et al. [22] first partition the city into even regions and then harnessed the power of CNN and LSTM in a joint model to capture the complex nonlinear relations of both space and time for taxi demand prediction. Very recently, to capture long-range spatial dependency from different city grids, a ConvPlus structure proposed by [14] showed the state-of-the-art performance in the prediction task. However, as detailed in Section 1, none of them considers the latent land function. Moreover, they are very inefficient in learning global context. To tackle these drawbacks, we present a general framework that can be easily generalized to all kinds of raster-based urban flow data in this paper.

5.2 Convolutional Neural Networks

During the past years, CNNs have made remarkable progress, especially in the field of computer vision. krizhevsky et al. first trained a large, deep CNN to classify the 1.2 million high-resolution images in the ImageNet LSVRC-2010 contest and won the first place [10]. Simonyan et al. further proposed the VGG-Net, in which they increased the network depth by using an architecture with very small (3×3) convolution filters [18]. However, training very deep CNNs are still difficult due to the gradient vanishing and exploding problems. To tackle this issue, an innovative study [3] first introduced a deep residual learning framework, which achieved great performance in many real-world applications. [6] proposed a densely connected CNN that can also alleviate this problem and encourage feature reuse. Recently, Hu et al. proposed a new unit named Squeeze-and-Excitation (SE) block [5], which can adaptively recalibrates channel-wise feature responses by explicitly modelling inter-dependencies between channels.

6 Conclusion and Future Work

In this paper, we have carefully investigated existing CNN-based methods for urban flow analytics, and exposed their inefficiency in capturing global context and incapability in generating region-specific predictions. Based on our discovery, we have presented the DeepLGR framework which decouples the local and global context extraction processes, and provides a parameter-efficient solution for customizing regional outputs. We have evaluated DeepLGR over two real-world urban flow analytics tasks, including citywide crowd flow prediction and fine-grained flow inference. Empirical results have not only demonstrated significant improvements on MAE and SMAPE over various strong baselines, but also the stability and generality of the presented framework. Moreover, our framework is more lightweight than the state-of-the-art methods, which is very important in real practice.

In the future, we will explore two probable directions. First, we notice that manually designing neural networks requires amount of expert efforts and domain knowledge. These designed models are always complicated with various spatio-temporal network modules where each module may have different network structures, which has limited their generality in other datasets. To overcome this problem, we plan to study Neural Architecture Search (NAS) for urban flow analytics, which can automatically construct a general neural network for diverse spatio-temporal tasks in cities. Second, since CNN architectures has inferiority in modeling graph data, we will extend our framework to a much broader set of spatio-temporal tasks by using graph convolutional networks.

References

1. Fan, Z., Song, X., Shibasaki, R., Adachi, R.: Citymomentum: an online approach for crowd behavior prediction at a citywide level. In: Proceedings of the 2015 ACM International Joint Conference on Pervasive and Ubiquitous Computing. pp. 559–569 (2015)
2. He, K., Zhang, X., Ren, S., Sun, J.: Spatial pyramid pooling in deep convolutional networks for visual recognition. *IEEE transactions on pattern analysis and machine intelligence* **37**(9), 1904–1916 (2015)
3. He, K., Zhang, X., Ren, S., Sun, J.: Deep residual learning for image recognition. In: Proceedings of the IEEE conference on computer vision and pattern recognition. pp. 770–778 (2016)
4. Hoang, M.X., Zheng, Y., Singh, A.K.: FCCF: forecasting citywide crowd flows based on big data. In: SIGSPATIAL. p. 6 (2016)
5. Hu, J., Shen, L., Sun, G.: Squeeze-and-excitation networks. In: Proceedings of the IEEE conference on computer vision and pattern recognition. pp. 7132–7141 (2018)
6. Huang, G., Liu, Z., Van Der Maaten, L., Weinberger, K.Q.: Densely connected convolutional networks. In: Proceedings of the IEEE conference on computer vision and pattern recognition. pp. 4700–4708 (2017)
7. Ioffe, S., Szegedy, C.: Batch normalization: Accelerating deep network training by reducing internal covariate shift. *arXiv preprint arXiv:1502.03167* (2015)
8. Kim, J., Kwon Lee, J., Mu Lee, K.: Accurate image super-resolution using very deep convolutional networks. In: Proceedings of the IEEE conference on computer vision and pattern recognition. pp. 1646–1654 (2016)
9. Kingma, D.P., Ba, J.: Adam: A method for stochastic optimization. *arXiv preprint arXiv:1412.6980* (2014)

10. Krizhevsky, A., Sutskever, I., Hinton, G.E.: Imagenet classification with deep convolutional neural networks. *Commun. ACM* **60**(6), 84–90 (May 2017)
11. Ledig, C., Theis, L., Huszár, F., Caballero, J., Cunningham, A., Acosta, A., Aitken, A., Tejani, A., Totz, J., Wang, Z., et al.: Photo-realistic single image super-resolution using a generative adversarial network. In: *Proceedings of the IEEE conference on computer vision and pattern recognition*. pp. 4681–4690 (2017)
12. Li, Y., Zheng, Y., Zhang, H., Chen, L.: Traffic prediction in a bike-sharing system. In: *Proceedings of the 23rd SIGSPATIAL International Conference on Advances in Geographic Information Systems*. pp. 1–10 (2015)
13. Liang, Y., Ouyang, K., Jing, L., Ruan, S., Liu, Y., Zhang, J., Rosenblum, D.S., Zheng, Y.: Urbanfm: Inferring fine-grained urban flows. In: *Proceedings of the 25th ACM SIGKDD International Conference on Knowledge Discovery & Data Mining*. p. 3132–3142 (2019)
14. Lin, Z., Feng, J., Lu, Z., Li, Y., Jin, D.: Deepstn+: Context-aware spatial-temporal neural network for crowd flow prediction in metropolis. In: *Proceedings of the AAAI Conference on Artificial Intelligence*. vol. 33, pp. 1020–1027 (2019)
15. Ouyang, K., Liang, Y., Liu, Y., Tong, Z., Ruan, S., Zheng, Y., Rosenblum, D.S.: Fine-grained urban flow inference. *arXiv preprint arXiv:2002.02318* (2020)
16. Pan, Z., Wang, Z., Wang, W., Yu, Y., Zhang, J., Zheng, Y.: Matrix factorization for spatio-temporal neural networks with applications to urban flow prediction. In: *Proceedings of International Conference on Information and Knowledge Management*. pp. 2683–2691 (2019)
17. Shi, W., Caballero, J., Huszár, F., Totz, J., Aitken, A.P., Bishop, R., Rueckert, D., Wang, Z.: Real-time single image and video super-resolution using an efficient sub-pixel convolutional neural network. In: *Proceedings of the IEEE conference on computer vision and pattern recognition*. pp. 1874–1883 (2016)
18. Simonyan, K., Zisserman, A.: Very deep convolutional networks for large-scale image recognition. *arXiv preprint arXiv:1409.1556* (2014)
19. Song, X., Zhang, Q., Sekimoto, Y., Shibasaki, R.: Prediction of human emergency behavior and their mobility following large-scale disaster. In: *Proceedings of the 20th ACM SIGKDD international conference on Knowledge discovery and data mining*. pp. 5–14 (2014)
20. Tucker, L.R.: Some mathematical notes on three-mode factor analysis. *Psychometrika* **31**(3), 279–311 (1966)
21. Xingjian, S., Chen, Z., Wang, H., Yeung, D.Y., Wong, W.K., Woo, W.c.: Convolutional lstm network: A machine learning approach for precipitation nowcasting. In: *Advances in neural information processing systems*. pp. 802–810 (2015)
22. Yao, H., Wu, F., Ke, J., Tang, X., Jia, Y., Lu, S., Gong, P., Ye, J., Li, Z.: Deep multi-view spatial-temporal network for taxi demand prediction. In: *Thirty-Second AAAI Conference on Artificial Intelligence* (2018)
23. Zhang, J., Zheng, Y., Qi, D.: Deep spatio-temporal residual networks for citywide crowd flows prediction. In: *Thirty-First AAAI Conference on Artificial Intelligence* (2017)
24. Zhang, J., Zheng, Y., Qi, D., Li, R., Yi, X.: DNN-based prediction model for spatio-temporal data. In: *SIGSPATIAL*. p. 92 (2016)
25. Zhao, H., Shi, J., Qi, X., Wang, X., Jia, J.: Pyramid scene parsing network. In: *Proceedings of the IEEE conference on computer vision and pattern recognition*. pp. 2881–2890 (2017)
26. Zheng, Y.: Trajectory data mining: an overview. *ACM Transactions on Intelligent Systems and Technology* **6**(3), 29 (2015)
27. Zheng, Y., Capra, L., Wolfson, O., Yang, H.: Urban computing: concepts, methodologies, and applications. *ACM Transactions on Intelligent Systems and Technology (TIST)* **5**(3), 1–55 (2014)
28. Zong, Z., Feng, J., Liu, K., Shi, H., Li, Y.: DeepDPM: Dynamic population mapping via deep neural network. In: *Proceedings of the AAAI Conference on Artificial Intelligence*. vol. 33, pp. 1294–1301 (2019)